

www.acsanm.org Article

Antibacterial Activity of Amphiphilic Janus Nanoparticles Enhanced by Polycationic Ligands

Jared T. Wiemann, Danh Nguyen, Swagata Bhattacharyya, Ying Li, and Yan Yu*



Cite This: ACS Appl. Nano Mater. 2023, 6, 20398-20409



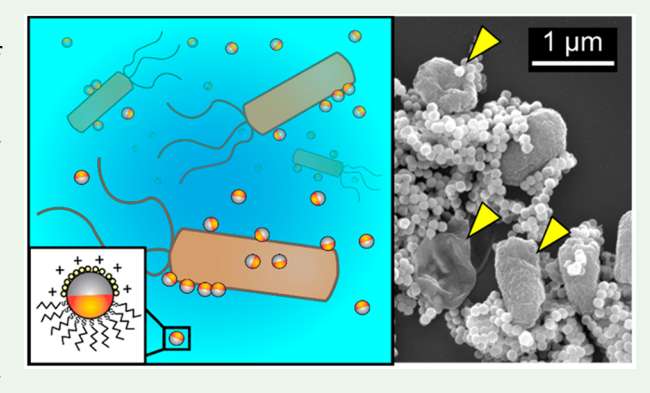
ACCESS

III Metrics & More

Article Recommendations

s Supporting Information

ABSTRACT: The rapid rise of antibiotic resistance has become a critical global health concern, necessitating the development of alternative treatments, such as antibacterial nanoparticles (NPs). While the antibacterial potency of these NPs is known to depend highly on their surface chemistry, existing designs predominantly include NPs with uniform surface coatings. In this study, we present a distinctive approach to using the surface anisotropy of NPs to modulate their antibacterial efficacy. Specifically, we investigate the antibacterial properties of amphiphilic Janus nanoparticles (NPs), which display spatially separated hydrophobic and cationic ligands on opposing sides. By integrating experiments with molecular dynamics simulations, we unveil the crucial role of polycationic ligands in enhancing the interaction between Janus NPs and bacteria, ultimately



leading to a significantly improved antibacterial potency. With hydrophobic and polycationic ligands spatially separated on a single NP surface, these amphiphilic Janus NPs effectively permeabilize the cell envelopes of both Gram-negative and Gram-positive bacteria. As a result, they inhibit bacterial growth at lower concentrations compared with NPs with uniform surface chemistry. Moreover, we demonstrate the versatility of the Janus NPs' antibacterial activity across various types of polycationic ligands. Our findings provide a mechanistic understanding of the spatial arrangement of ligands as well as the molecular characteristics of ligands in modulating NP-bacteria interactions. This research underscores the potential of Janus NPs, a distinctive subgroup of nanoparticles characterized by their anisotropic surface chemistry, as a unique class of antibacterial materials.

KEYWORDS: antibiotic resistance, Janus nanoparticles, surface anisotropy, antibacterial materials, amphiphilic nanoparticles

■ INTRODUCTION

The rapid rise of antibiotic-resistant bacteria is a growing public health concern, as the development of new antibiotics lags behind the emergence of multidrug-resistant strains. In the United States alone, there are approximately 2.8 million cases of antibiotic-resistant infections each year, resulting in around 35,000 deaths. This alarming trend highlights the urgent need for new therapeutics. Nanoparticles (NPs) have emerged as a promising alternative to traditional antibiotics because they act through antimicrobial mechanisms less likely to cause acquired drug resistance. 2-7

Various types of antibacterial nanomaterials, including metal and metal oxide NPs, liposomes, and polymeric NPs, have been developed. These nanomaterials exert their antibacterial effects through different mechanisms, such as DNA binding, ^{8–10} oxidative stress induction, ^{11,12} direct penetration of bacterial membranes, ^{13–15} and adhesion-induced mechanical rupture of cell walls. ¹⁶ However, the physical interaction between NPs and bacteria, which is highly influenced by the surface chemistry of NPs, is a crucial factor in their effectiveness. Cationic NPs, in particular, have been shown to strongly bind to both Gram-negative and Gram-positive

bacteria due to electrostatic attraction to the highly anionic bacterial surface. 17,18 Nevertheless, there is ongoing debate regarding whether NP binding to bacterial surfaces correlates with their efficiency in killing bacteria. $^{19-21}$

To enhance the antibacterial potency of NPs, researchers have explored surface coatings consisting of mixtures of different ligands. Studies have demonstrated that NPs functionalized with a combination of cationic and hydrophobic ligands are more effective in damaging bacterial cell membranes and inhibiting bacterial growth compared to those coated solely with cationic ligands. Moreover, modifying the chain length and functional end groups of amphiphilic surface capping ligands has been shown to modulate the antibacterial properties of the coated NPs. 22,25,26 These findings suggest that achieving an optimized

Received: September 21, 2023 Revised: September 29, 2023 Accepted: October 4, 2023 Published: October 20, 2023





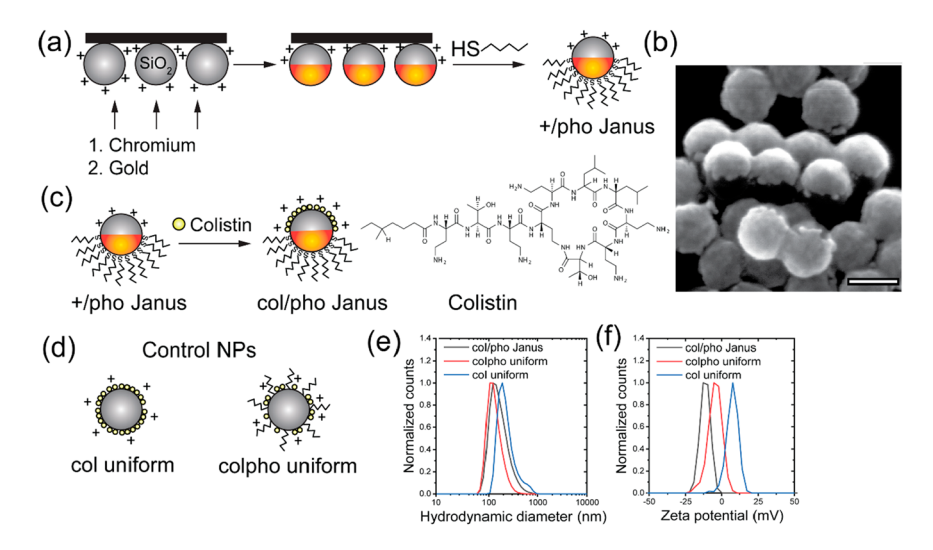


Figure 1. Fabrication and characterization of NPs. (a) Fabrication of monocationic/hydrophobic (+/pho) Janus NPs. (b) SEM image of +/pho Janus NPs. Scale bar: 100 nm. (c) Fabrication of colistin/hydrophobic (col/pho) Janus NPs and the molecular structure of colistin. (d) Illustration of two control NPs coated with a uniform coating of colistin only (col uniform) or a mixture of colistin and hydrophobic alkyl ligands (colpho uniform). (e, f) Hydrodynamic diameter and zeta potential of different types of NPs in 2 mM HEPES (pH 7.2).

balance between hydrophobicity and cationic charge on NPs is essential for their antimicrobial activity. However, all of those studies focused on uniformly coated NPs. The disadvantage of having a uniform coating of different ligands is that it can create energetic barriers that hinder the NP interaction with membranes. While cationic charges facilitate NP binding to membranes, they can impede membrane penetration driven by hydrophobicity. ^{27–32}

In this study, we present a distinct approach by spatially separating the hydrophobic and cationic moieties on a single NP. We hypothesized that this spatial separation allows NPs to be attracted to lipid bilayers through electrostatic interactions without interference from the hydrophobic ligands. Subsequently, the NPs can insert into biomembranes from their hydrophobic hemisphere without hindrance from the charged hemisphere.²⁸ Our previous work using model lipid membranes has shown that Janus NPs, which possess this spatial separation, are more effective in disrupting lipid membranes compared to uniform NPs. 27-30,33 Building upon this knowledge, we ask: does the spatial separation of hydrophobicity and cationic charges on Janus NPs enhance their interaction with and killing of bacteria? To address this question, we combined experimental approaches with molecular dynamics (MD) simulations. Through our research, we not only provide an answer to this question but also shed light on the crucial role of polycationic ligands in promoting NP-bacteria interactions and enhancing the antibacterial potency of Janus NPs.

Our results demonstrate that amphiphilic Janus NPs, which bear separate polycationic and hydrophobic ligands on opposite sides, effectively permeabilize the cell envelopes of both Gram-negative and Gram-positive bacteria. Remarkably, these NPs inhibit bacterial growth at extremely low concentrations in the picomolar range, which is more effective than uniformly coated NPs. MD simulations further reveal that the polycationic ligands enable strong electrostatic attractions between the NPs and the negatively charged lipopolysaccharides (LPS) on bacterial membranes. Consequently, the hydrophobic side of the NPs can interact with the hydrophobic core of the lipid membranes, ultimately leading to membrane disruption. We confirm the versatility of the Janus NPs'

antibacterial activity across various types of polycationic ligands. In addition to demonstrating the effectiveness of antibacterial Janus NPs, our work sheds light on the mechanism by which the spatial arrangement and molecular characteristics of the ligands influence interactions between Janus NPs and bacteria.

■ RESULTS AND DISCUSSION

Design and Characterization of Amphiphilic Janus NPs. In previous studies, we have demonstrated the effectiveness of amphiphilic Janus nanoparticles (NPs), which possess cationic and hydrophobic properties on opposite sides, in inducing pores in model lipid membranes.^{27–30,33} Based on these findings, we initially hypothesized that these Janus NPs could also disrupt the outer membrane of bacteria. To test this hypothesis, we synthesized the Janus NPs (termed +/pho Janus NPs) by coating one hemisphere of aminated silica NPs with thin layers of chromium and gold. We then conjugated octadecanethiol on the gold coating to render the hemisphere hydrophobic (Figure 1a). The Janus geometry of these NPs was confirmed by using scanning electron microscopy (Figure 1b). To evaluate the interaction of the +/pho Janus NPs with bacterial membranes, we incubated them at various concentrations with Escherichia coli (E. coli, MG1655 strain) for 2 h at 37 °C with shaking. The integrity of the bacterial cell wall was assessed by using the propidium iodide assay. Propidium iodide is a DNA stain that is weakly fluorescent in water but becomes strongly fluorescent upon diffusion into bacteria with permeabilized cell envelopes. Surprisingly, we observed only a minimal increase in propidium iodide staining in E. coli in the presence of +/pho Janus NPs, even at concentrations up to 300 pM (Figure S1). Estimating the percentage of bacteria with intact cell wall based on the intensity of staining, we found no significant impact from the +/pho Janus NPs (Figure S1C). We further confirmed that the propidium iodine assay was not affected by the imaging buffer used (Figure S2).

Considering our previous understanding that the +/pho Janus NPs are attracted to model lipid membranes through electrostatic interactions, we speculated that the monocationic ligands (primary amine from (3-aminopropyl)triethoxysilane)

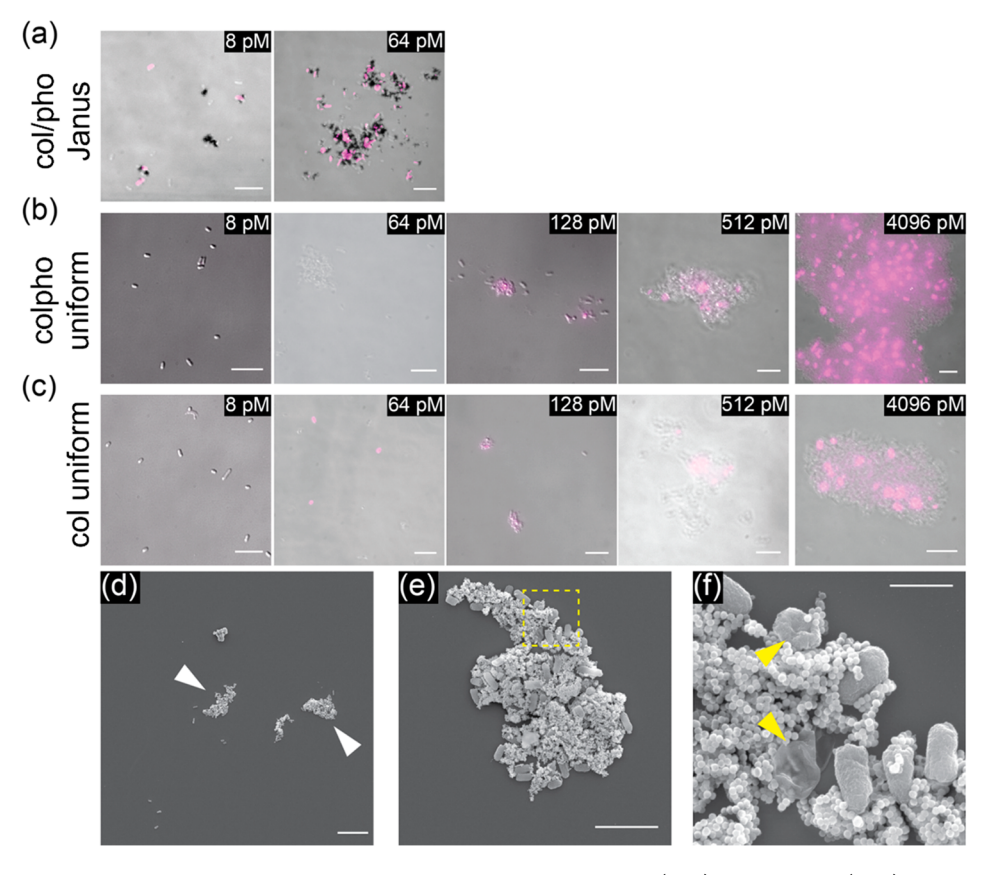


Figure 2. Permeabilization of *E. coli* cell envelopes induced by colistin-functionalized NPs. (a–c) Merged DIC (gray) and fluorescence (magenta) images of *E. coli* stained with propidium iodide after incubation with various concentrations of (a) col/pho Janus NPs, (b) colpho uniform NPs, and (c) col uniform NPs. Scale bars: 10 μ m. (d–f) SEM image of *E. coli* after interaction with 128 pM col/pho Janus NPs. Arrows indicate the large aggregation of col/pho JPs and *E. coli* cells. Panel (f) is a zoomed-in picture of the boxed area in (e). Scale bars: 10 μ m in panel (d), 5 μ m in panel (e), and 1 μ m in panel (f).

on these NPs might not provide sufficient electrostatic attraction to the bacterial membrane, thus encountering a steric barrier posed by the bulky lipopolysaccharides (LPS). This led us to question whether replacing the monocationic ligands with polycationic ones could enhance the interaction of the Janus NPs with bacterial membranes. One potential candidate for the polycationic ligands we considered was colistin, a cationic polypeptide with five primary amines and 11 secondary amines (Figure 1c). Colistin is a polymyxin antibiotic used as a "last resort" therapy against multidrug resistant Gram-negative bacteria. ^{34,35} We aimed to replace the primary amines on the +/pho Janus NPs with colistin to create Janus NPs that are hydrophobic on one hemisphere and coated with colistin on the other (termed col/pho Janus NPs).

To prepare the NPs, we conjugated colistin to the +/pho Janus NPs using glutaraldehyde, which cross-linked the primary amine groups on the +/pho Janus NPs with the L-diaminobutyric acid residues in colistin (Figure 1c). We also fabricated two types of control NPs to investigate the effects of the anisotropic presentation of surface ligands (Figure 1d). One type involved uniformly coating colistin on aminated silica NPs without hydrophobic ligands on the surface, known as colistin uniform NPs (col uniform NPs). The other type, termed colistin hydrophobic uniform NPs (colpho uniform NPs), had a uniform coating of a mixture of colistin and the hydrophobic ligand octadecyltrimethoxysilane, which contains the same alkyl chain as the octadecanethiol on the Janus NPs. As expected, the conjugation of hydrophobic ligands resulted

in slightly decreased zeta potentials of the col/pho Janus NPs and colpho uniform NPs, confirming the successful ligand conjugation on the different NPs (Figure 1e,f).

Permeabilization of E. coli Cell Envelop by Colistin-**Coated NPs.** To test our hypothesis that polycationic ligands enhance the interaction of Janus NPs with bacterial membranes, we examined the effect of the NPs on the integrity of the *E. coli* cell envelope using the propidium iodide assay, as described previously for the +/pho Janus NPs. In our experiments, we localized the bacteria and NPs using differential interference contrast (DIC) microscopy and identified bacteria with permeabilized cell walls by combining DIC with fluorescence images of propidium iodide staining (Figure 2a-c). We observed that the col/pho Janus NPs induced noticeable permeabilization in the bacterial cell wall at an 8 pM concentration, and the extent of permeabilization significantly increased at a 64 pM NP concentration. Interestingly, at this higher NP concentration, the col/pho Janus NPs and E. coli formed large aggregates (Figure 2a). These Janus NP-bacteria aggregates could reach sizes of tens of micrometers in diameter. Using SEM, we further observed that many Janus NPs were bound to and aggregated around E. coli cells (Figure 2d-f). Many bacteria exhibited deformations, including indentations in their cell walls, and some had collapsed cell structures (Figure 2f). Because large cell-particle aggregates scatter light intensely and emit fluorescence levels significantly higher than those of single

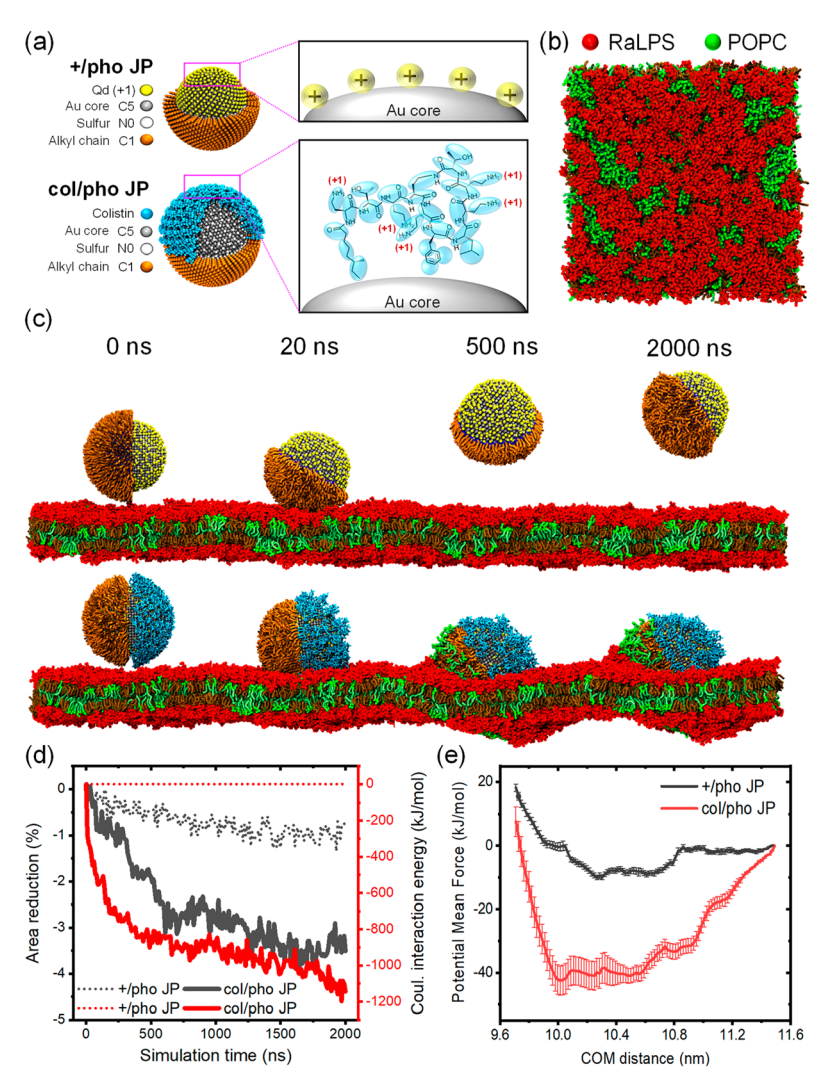


Figure 3. CGMD simulations of interactions of +/pho Janus NP and col/pho Janus NP with the model bacterial membrane (RaLPS/POPC). (a) CG representations of the +/pho Janus NP and col/pho Janus NP in MD simulation models. Coloring scheme: Janus NP model contains Au core (gray), sulfur (white), cationic ligand (yellow), hydrophobic ligand (orange) beads, and CG representations of colistin (cyan). Core diameter of Janus NP is 10 nm. (b) Snapshot of the RaLPS/POPC membrane (top view) after a full relaxation. (c) Representative snapshots (side views) showing the interaction of +/pho Janus NP (top) and col/pho Janus NP (bottom) with RaLPS/POPC membrane. The total simulation time is 2.00 μ s. Membrane dimension: ~ 30 × 30 nm². Solvent molecules are included in the simulation, but not shown for clarity. (d) Left-side y-axis: the total projected area reduction (%) of RaLPS/POPC membrane plotted as a function of time in the presence of +/pho Janus NP and col/pho Janus NP. Right-side y-axis: the electrostatic interaction energy (Coulomb interaction) of +/pho Janus NP and col/pho Janus NP with the RaLPS/POPC membrane during the simulation. (e) Potential mean force calculation of the interaction of +/pho Janus NP and col/pho Janus NP with the RaLPS/POPC membrane.

bacteria, flow cytometry was unsuitable for quantifying the percentage of membrane-intact bacteria.

To ascertain whether the NPs induced damage solely to the outer membrane or affected both the outer and inner membranes of bacteria, we employed double-staining of vancomycin-BODIPY and propidium iodine. Vancomycin-BODIPY is a fluorescently labeled glycopeptide antibiotic that labels the peptidoglycan once the outer membrane is permeabilized. Following incubation of *E. coli* with Janus NPs (64 pM) and colpho uniform NPs (512 pM), we observed that more *E. coli* cells were stained with vancomycin-BODIPY compared to those stained with propidium iodine (Figure S3). This discrepancy indicated heterogeneous disruption of the *E. coli* cell envelope by the NPs, affecting both outer and inner membranes in some bacteria while affecting only the outer membrane in others. Notably, we

observed that the vancomycin-BODIPY labeling of the *E. coli* strain we used is highly sensitive to the staining conditions, particularly the incubation temperature and dye concentrations. This is consistent with previously reported observations. ^{36,37} Consequently, these experiments need careful optimization and execution of control experiments.

Those findings together starkly contrast with our observation that the +/pho Janus NPs failed to induce cell envelope disruption in *E. coli* even at concentrations as high as 300 pM. The observed difference supports our speculation that replacing the primary amine groups with the polycationic ligand colistin enhances the interaction of Janus NPs with bacterial membranes and the NP-induced disruption to the bacterial cell envelope.

Compared to the col/pho Janus NPs, the col uniform NPs and colpho uniform NPs induced damage to the bacterial cell

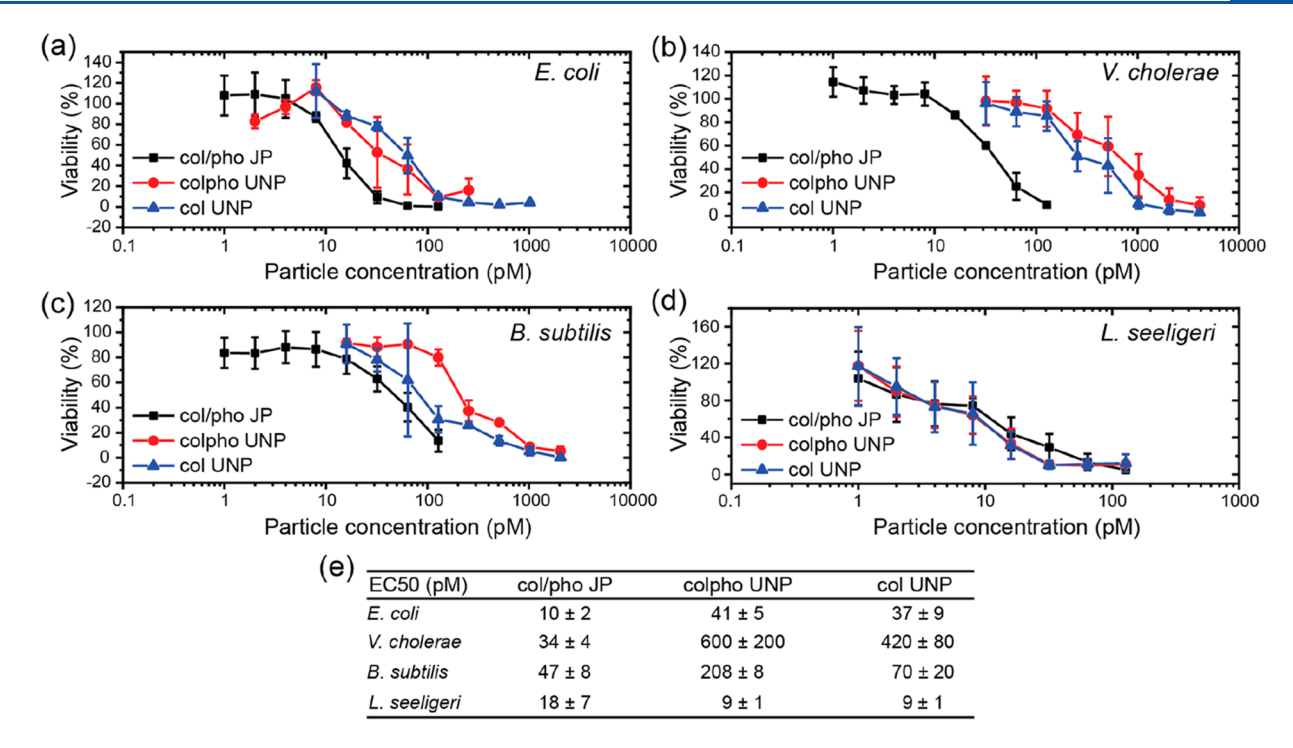


Figure 4. Effect of colistin-functionalized NPs on bacterial viability measured by using a growth-based viability assay. Viability of Gram-negative bacteria, *E. coli* (a) and *V. cholerae* (b), and Gram-positive bacteria, *B. subtilis* (c) and *L. seeligeri* (d), in the presence of col/pho Janus NP, colpho uniform NPs, and col uniform NPs. (e) EC50 for each type of NPs and bacteria obtained from data in (a–d).

envelope at much higher concentrations (Figure 2b,c). Interestingly, the presence of large NP-bacteria aggregates, within which a significant fraction of bacteria were stained with propidium iodide, was also observed in the presence of 512 pM colpho uniform NPs or 4096 pM col uniform NPs. This comparison demonstrates that when NPs possess sufficient cationic charges on the surface, the addition of surface hydrophobicity renders them more effective in permeabilizing the cell envelopes of *E. coli*. Among the three types of NPs tested, the col/pho Janus NPs exhibited the highest potency. This prompts the question: How does polycationic ligand colistin enhance the Janus NP-bacterial membrane interaction?

Simulation of the Effect of Col/Pho Janus NPs on Bacterial Outer Membranes. We next employed Coarse-Grained Molecular Dynamics (CGMD) simulations to gain insight into how polycationic ligand colistin enhances the interaction between Janus NPs and bacterial outer membranes. Figure 3a depicts the Janus NP designs in the CGMD model based on the MARTINI force field.³⁸ The +/pho Janus NPs were modeled with a gold core (C5 beads) that featured two hemispheres separately coated with hydrophobic or cationic ligands, based on our previous studies. 30,33 The hydrophobic ligand, octadecyl, was modeled with an 18-C alkyl chain (four MARTINI CG C1 beads), while the monocationic primary amine ligand was modeled with a single positive bead (+1 Qd). In comparison, the col/pho Janus NPs incorporated colistin as the polycationic ligand, modeled with multiple positive beads, while the hydrophobic ligand was the same as that for the +/pho Janus NPs. The bead types for colistin were derived from Lei Fu et al.,³⁹ and each colistin molecule consisted of five monopositive beads.

The MD model included a lipid membrane composed of 40 mol $\,\%\,$ RaLPS (rough lipopolysaccharides) and 60 mol $\,\%\,$

POPC (Figure 3b). At this composition, the surface coverage of RaLPS is 75%, which represents the reported value in Gramnegative bacterial outer membranes. To initiate the simulations, we positioned the Janus NP of interest above the lipid membrane with the interface separating the hydrophobic and cationic hemispheres perpendicular to the membrane plane (Figure 3c at 0 ns). After energy minimization to eliminate steric clashes and relax the system, we pulled the Janus NP toward the membrane and restrained it at a center-of-mass (COM) distance of 6.0 nm from the bacterial membrane. This pulling, conducted over 100 ns, facilitated initial interactions between the Janus NP and the membrane. At 20 ns, we observed a slight rotation of the +/pho Janus NP when it approached the membrane, while the col/pho Janus NP maintained its initial orientation and exhibited stronger adhesion to the membrane. We subsequently released the restraint and conducted additional dynamics for up to 2.0 μ s. In the later stages of the simulation, the col/pho Janus NP caused significant membrane disruption, including the extraction of lipid molecules from the membrane. In contrast, the +/pho Janus NP detached from the membrane quickly after 500 ns and thus did not cause any lipid extraction or disruption to the membrane (Figure 3c, Video S1, and Video S2).

For a quantitative comparison of NP-induced membrane disruption, we observed that the col/pho Janus NP resulted in a significant reduction in membrane area, nearly a 4-fold increase compared to the +/pho Janus NP (Figure 3d). Furthermore, the col/pho Janus NP exhibited substantial electrostatic interaction with the membrane, while the +/pho Janus NP did not. To evaluate the binding energy between the different Janus NPs and the bacterial membrane, we employed the umbrella sampling technique⁴¹ and extracted the potential mean force (PMF) as a function of the distance between the

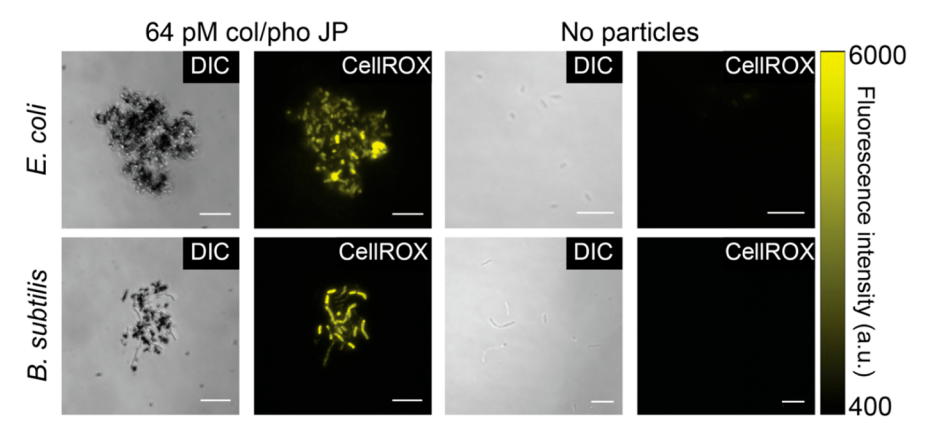


Figure 5. ROS generation in *E. coli* and *B. subtilis* induced by col/pho Janus NPs. Differential interference contrast (DIC) and epifluorescence images of *E. coli* (top) and *B. subtilis* (bottom) labeled with CellROX in the presence or absence of 64 pM col/pho Janus NPs. Scale bars: 10 µm.

NP's COM and the middle plane of the membrane (Figure 3e). The results indicated that the col/pho Janus NP had a significantly lower binding energy ($\sim -40 \text{ kJ/mol}$) compared to the +/pho Janus NP ($\sim -10 \text{ kJ/mol}$), consistent with the stronger electrostatic interaction.

The simulation results support our experimental observations that the presence of the polycationic ligand colistin on Janus NPs promotes their interaction with bacterial membranes and subsequent membrane disruption. The unique structural characteristics of colistin, with multiple cationic charges displayed on a branched molecular backbone, enable effective electrostatic interactions between the NPs and the negatively charged outer and inner core oligosaccharides of LPS on the bacterial membrane (Figure 3d). Driven by the strong electrostatic attraction toward the membrane, the hydrophobic hemisphere of the NP approaches the hydrophobic core of the lipid membrane, leading to membrane disruption. This thermodynamic advantage is not observed with monocationic ligands.

Effect of Janus NPs on Bacterial Viability. Having confirmed that the col/pho Janus NPs damage the E. coli cell envelope at concentrations as low as 8 pM, we further investigated their antibacterial activity against two Gramnegative bacterial strains (E. coli and V. cholerae) and two Gram-positive bacterial strains (B. subtilis and L. seeligeri). We also compared the antibacterial effect of the Janus NPs to those of the two types of control NPs to analyze the impact of anisotropic ligand presentation. We employed a growth-based viability assay developed by Qiu et al.⁴⁰ to evaluate the effect of the NPs on bacterial growth. Commonly used high-throughput optical assays have limitations in evaluating the antibacterial activity of NPs due to the strong optical interference caused by NPs and the aggregation issue of NPs in nutrient-rich medium. This growth-based viability assay mitigates those limitations by diluting the exposure media containing bacteria and NPs into fresh growth media. Figure 4 shows the viability (%) of each bacterial strain as a function of the NP concentration. By fitting the dose-response plots with Boltzmann-sigmoidal curves, we estimated the half maximal effective concentrations (EC50) for each type of bacterial strain and NP. We found that the col/ pho Janus NPs at pM concentrations effectively inhibited the growth of both Gram-positive and Gram-negative bacteria in all four strains tested. Compared to col/pho uniform NPs or colistin uniform NPs, the col/pho Janus NPs exhibited greater potency in inhibiting bacterial growth, with the exception of the Gram-positive bacterium *L. seeligeri*, which appeared highly sensitive to all three types of NPs.

The viability results yielded intriguing findings. First, among all three types of NPs, the col/pho Janus NPs exhibited the highest potency in inhibiting bacterial growth. Although the surface hydrophobicity of NPs only slightly increased their antibacterial effect, as observed in the col/pho uniform NPs and col uniform NPs, the most significant effect stemmed from the spatial segregation of cationic charges and hydrophobic ligands on the Janus NP surfaces. It is plausible that when colistin and the hydrophobic ligand are uniformly mixed on NP surfaces, the proximity of the hydrophobic ligand to colistin hinders the electrostatic attraction between the NPs and the bacterial membrane. Conversely, the proximity of colistin to the hydrophobic ligands impedes hydrophobicitydriven membrane disruption. This effect is absent in the case of col/pho Janus NPs, where the two ligands are spatially segregated. Second, colistin-coated NPs, whether Janus or uniform, exhibited much higher potency against Gram-negative bacteria compared to soluble colistin, which had an EC50 of approximately 1 μ M for both E. coli and V. cholera (Figures S4 and S5). Surprisingly, all three types of colistin-coated NPs also inhibited the growth of Gram-positive bacteria in our study, despite soluble colistin having minimal inhibitory effects on Gram-positive bacteria. Overall, the col/pho Janus NPs proved to be the most effective against both Gram-negative and Gram-positive bacteria.

The viability results align with our observations from the propidium iodine assay, confirming that the col/pho Janus NPs inhibit bacterial growth at lower concentrations than the uniform NPs. The propidium iodide data indicate that disrupting the cell envelope is a major antibacterial mechanism of action for the Janus NPs. To further validate this mechanism for Gram-positive bacteria, which were effectively inhibited by col/pho Janus NPs, we examined the effect of these NPs on the cell envelope of Gram-positive bacterium B. subtilis. Similar to our observations with E. coli, col/pho Janus NPs (64 pM) induced substantial permeabilization of the cell wall in B. subtilis, leading to the formation of large aggregates with the NPs (Figure S6a). In comparison, B. subtilis without NP treatment remained well dispersed (Figure S6b). This intriguing observation is noteworthy because, unlike Gramnegative bacteria, Gram-positive bacteria lack an outer membrane but possess a thick layer of highly anionic peptidoglycan. The col/pho Janus NPs effectively disrupted both types of bacterial envelope structures. Additionally, the

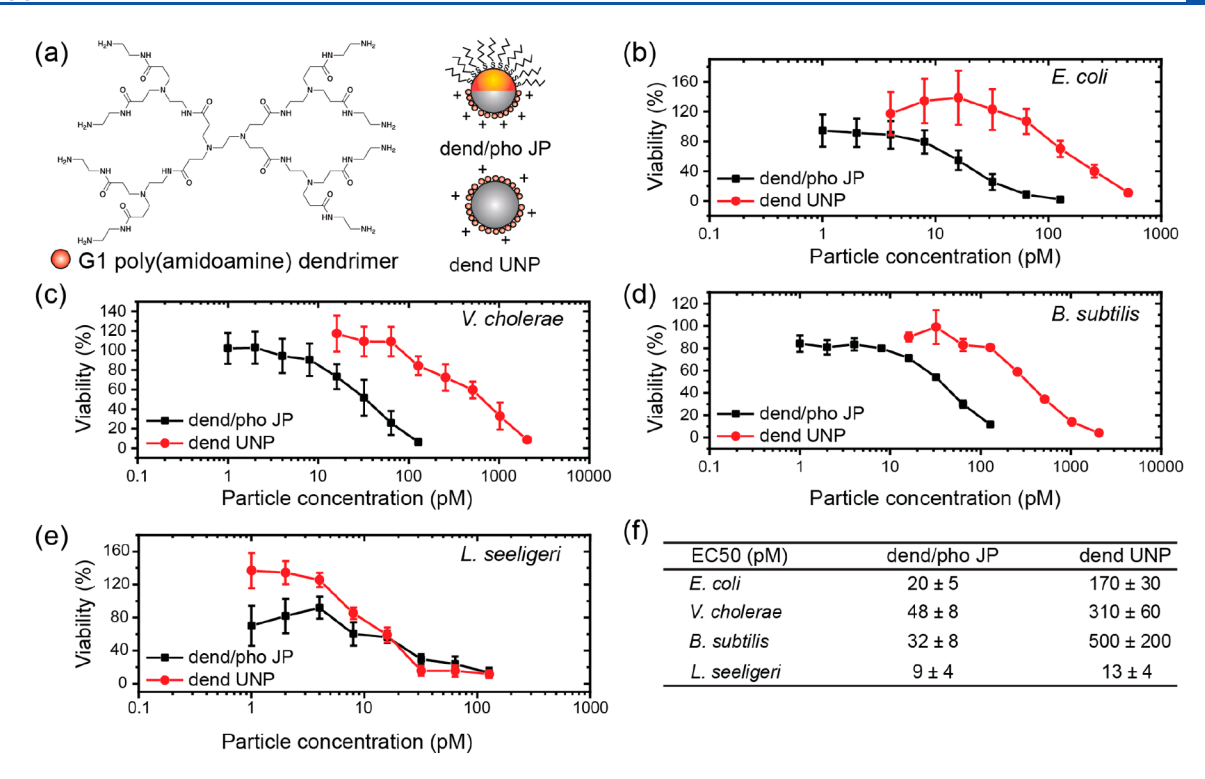


Figure 6. Effect of dendrimer-functionalized NPs on bacterial viability measured using a growth-based viability assay. (a) Chemical structure of a generation 1.0 PAMAM dendrimer and schematic of two types of dendrimer-functionalized particles used in these experiments: dend/pho Janus NP and dend uniform NP. (b–e) Viability of Gram-negative bacteria, *E. coli* (a) and *V. cholerae* (b), and Gram-positive bacteria, *B. subtilis* (c) and *L. seeligeri* (d), in the presence of different types of NPs. (f) EC50 for each type of NPs and bacteria obtained from data in (b–e).

exact mechanisms underlying the extensive aggregation of bacteria, both *E. coli* and *B. subtilis*, caused by the col/pho Janus NPs remain unknown. One plausible explanation is that bacteria form aggregates to survive unfavorable growth conditions, as previously reported for clumps of bacteria with damaged cell walls induced by oxidative stress.⁴¹ This explanation aligns with our observation that bacterial aggregation was more pronounced at higher NP concentrations.

Because soluble colistin has been shown to induce reactive oxygen species (ROS) in Gram-negative species, such as A. baumannii,42 we next examined whether the col/pho Janus NPs induce reactive oxygen species (ROS) in bacteria, in addition to membrane permeabilization. We used CellROX Deep Red, a fluorogenic ROS indicator that becomes intensely fluorescent upon reacting with ROS. Bacterial samples were incubated with 64 pM col/pho Janus NPs for 2 h and subsequently stained with CellROX. As shown in Figure 5, both E. coli and B. subtilis exhibited strong CellROX fluorescence in the presence of col/pho Janus NPs, indicating ROS generation induced by the NP interaction. Bacteria within the large aggregates displayed stronger fluorescence compared to that of isolated bacteria. These results confirm that col/pho Janus NPs induce elevated ROS production in both E. coli and B. subtilis.

Generality of the Effectiveness of Polycationic/ Hydrophobic Janus NPs. After confirming the effectiveness of col/pho Janus NPs against both Gram-negative and Grampositive bacteria, we aimed to determine whether the NP potency was specifically due to the antibiotic effect of colistin or the general outcome of the polycationic effect. To address this question, we replaced colistin with a polycationic PAMAM

dendrimer on the Janus NPs while keeping the hydrophobic ligand unchanged. Although dendrimer molecules have been demonstrated to kill bacteria, 43 they are not used as antibiotics in clinical applications. We opted for the generation 1.0 PAMAM dendrimer as it possesses a molecular weight similar to that of colistin and a comparable number of cationic charges, with eight primary amines compared to the seven primary amines in colistin (Figure 6a). We prepared hydrophobic/dendrimer-coated Janus NPs (dend/pho Janus NPs) and uniform dendrimer NPs (dend uniform NPs) as control samples. Hydrodynamic diameter measurements of the dendrimer NPs indicated that the particles were well dispersed following functionalization (Figure S7a). The zeta potentials were $+10 \pm 2$ and $+25 \pm 2$ mV for dend/pho Janus NPs and dend uniform NPs, respectively (Figure S7b). Viability assays were performed using the same panel of four bacterial types as used for col/pho Janus NPs, and similar trends were observed. We confirmed that dend/pho Janus NPs, like col/pho Janus NPs, effectively inhibited the growth of both Gram-negative and Gram-positive bacteria at pM concentrations (Figure 6be). The EC50 values calculated from the dose—response curves in Figure 6b-e revealed that Janus NPs were approximately 4 and 16 times more potent than uniform NPs against E. coli and B. subtilis, respectively (Figure 6f). These results collectively support the finding that amphiphilic Janus NPs are generally more potent in inhibiting bacterial growth than uniform NPs. The increased antibacterial potency of Janus NPs is predominantly attributed to the anisotropic presentation of both hydrophobic and polycationic ligands on a single particle surface, as demonstrated in our simulation results, rather than the intrinsic antibiotic activity of the ligand itself.

CONCLUSION

In this study, we investigated the antibacterial activities of amphiphilic Janus NPs with unique surface chemistryhydrophobic on one side and cationic on the other. Our approach integrated experimental investigations and molecular dynamics (MD) simulations to unveil the pivotal role of polycationic ligands as opposed to monocationic ligands in promoting NP-bacteria interactions and enhancing the antibacterial potency of the NPs. Remarkably, our findings hold true across a range of polycationic ligands, including colistin, the polymyxin antibiotic, and a nonantibiotic polyamidoamine dendrimer. Our results demonstrate that amphiphilic Janus NPs, bearing either of the aforementioned polycationic ligands, effectively permeabilize the cell envelopes of both Gram-negative and Gram-positive bacteria, inhibiting bacterial growth at astonishingly low concentrations in the picomolar range. Through MD simulations, we discovered that the polycationic ligands facilitate strong electrostatic attractions between the NPs and the negatively charged sugar cores of lipopolysaccharides (LPS) on the bacterial membrane. This effectively reduces the binding energy of the Janus NPs to the bacterial membrane and allows the hydrophobic side of the NPs to interact with the hydrophobic core of the lipid membrane, ultimately leading to membrane disruption. Moreover, the spatial separation of the hydrophobic and polycationic ligands on the Janus NPs confers significantly increased potency compared with NPs with a uniform surface chemistry. This study represents a significant step forward in understanding the mechanisms underlying the antibacterial activities of Janus NPs and lays the foundation for the rational development of these NPs for antibacterial applications. Our findings opened doors to many questions to explore in future studies, including the biocompatibility and potential cytotoxicity of Janus NPs.

MATERIALS AND METHODS

Cells and Reagents. E. coli (MG1655), L. seeligeri (RR4), and B. subtilis (SB168) were generously provided by Prof. J. P. Gerdt at Indiana University-Bloomington. Avirulent V. cholerae El Tor O1 strain was engineered and kindly gifted by Prof. Andrew Camilli at Tufts University. Luria-Bertani (LB) agar, Luria broth base, and CellROX Deep Red Reagent (termed CellROX) were purchased from Invitrogen (Waltham, MA). Brain heart infusion broth and brain heart infusion agar were purchased from Thermo Fisher Scientific. Aminefunctionalized silica NPs (100 nm) were procured from Nanocomposix (San Diego, CA). Gold (99.99% purity) and chromium (99.99% purity) were purchased from Kurt J. Lesker et al. (Jefferson Hills, PA). Octadecanethiol, propidium iodide, octadecyltrimethoxysilane, colistin sulfate, G1 poly(amidoamine) dendrimer (20 wt % in methanol), and HEPES were purchased from Sigma-Aldrich (St. Louis, MO). Vancomycin-BODIPY was purchased from Thermo Fisher. Ultrapure water (18 $M\Omega\cdot cm$) was used for all experiments.

Nanoparticle Fabrication and Characterization. Amphiphilic cationic Janus NPs were fabricated as previously described. ²⁸ Cationic silica NPs (100 nm in diameter) were drop cast onto piranha etched microscope slides to make a submonolayer of particles. An Edwards thermal evaporation system (Nanoscale Characterization Facility at Indiana University) was used to sequentially deposit thin layers of chromium (5 nm) and gold (25 nm) onto one hemisphere of the NPs. Particle monolayers were immediately immersed in 2 mM 1-octadecanethiol for at least 12 h before use to make the gold caps on the particles hydrophobic. Particles were sonicated from microscope slides and subjected to differential centrifugation (4 times at 100g and 4 times at 500g) to remove metal bridging aggregates formed during

thermal evaporation. Janus particle gold coating was assessed by scanning electron microscopy (Nanoscale Characterization Facility at Indiana University). Amphiphilic silica NPs were prepared prior to colistin conjugation. Briefly, octadecyltrimethoxysilane and 1 M HCl were added dropwise to THF to prepare a solution containing 22 mM octadecyltrimethoxysilane and 0.6 vol % of HCl. Cationic silica NPs were resuspended in 8:1 (v/v) hexanes:octadecyltrimethoxysilane solution with vigorous stirring for 1 h at room temperature. The resulting amphiphilic silica NPs were washed 3 times with ethanol and 3 times with water before further surface modification.

To conjugate PAMAM dendrimer or colistin, NPs (amphiphilic Janus NPs, amphiphilic cationic silica particles, or cationic silica NPs) were washed 3 times with 10 mM HEPES buffer (pH 7.4) and resuspended with 10% glutaraldehyde in 10 mM HEPES buffer for 90 min at room temperature with gentle rotation. After glutaraldehyde activation of the amine groups on the particle surface, the particles were washed three times with 10 mM HEPES buffer to remove excess glutaraldehyde. Particles were then resuspended with colistin or a PAMAM dendrimer (1 mg/mL in 10 mM HEPES buffer) for 60 min at room temperature with gentle rotation. Particles were washed three times again with 10 mM HEPES followed by three times washing with 2 mM HEPES 25 mM NaCl buffer to remove unreacted colistin or the PAMAM dendrimer. Particles were stored at 4 °C until use. Hydrodynamic radius and zeta potential of all particles were characterized using a Malvern Zetasizer instrument (Nanoscale Characterization Facility at Indiana University). The concentration of particles was measured using a Particle Metrix ZetaView (Nanoscale Characterization Facility at Indiana University).

Growth-Based Viability Assay. Colonies of bacteria (E. coli MG1655, avirulent V. cholerae, and B. subtilis SB168) were grown by streaking frozen glycerol:water stocks onto an LB agar plate and incubating the plate for 24 h at 37 °C. Three colonies from the agar plate were then suspended in Luria broth to make stock suspensions, and the bacteria were grown to stationary phase overnight at 37 °C with constant shaking. L. seeligeri RR4 was grown using a brain heart infusion agar plate and brain heart infusion broth with the same protocol. Bacteria were then washed three times with 0.85% NaCl followed by three washes with 2 mM HEPES 25 mM NaCl (pH 7.2) immediately before each experiment. The growth-based viability assay, which determines bacteria viability based on the onset of logarithmic bacterial growth after exposure to a nanomaterial, was performed with modification as described by Qiu et al.⁴⁰ The exposure plate was made by making serial dilutions of NPs suspended in 2 mM HEPES, and 25 mM NaCl was performed on a 96-well plate. Bacteria were added to each well with particles for a final concentration of 1×10^7 cfu/mL (4 × 10^7 for B. subtilis and L. seeligeri). Two rows on each 96-well plate containing bacteria without NPs were used to generate a calibration curve of the viability. In each row, 1×10^7 cfu/mL (4 × 10⁷ for *B. subtilis* and *L. seeligeri*, treated as 100% viability) was added to the first well, and serial dilutions were performed in the subsequent wells. A row of wells with only media was added to each plate as a control for media sterility. The exposure plate was incubated for 2 h at 37 °C with 280 rpm shaking. After incubation, 20 μ L of each well from the exposure plate was transferred into 180 µL each of growth media in a new 96-well plate (M9 minimal media for E. coli and V. cholerae, Luria broth for B. subtilis, and brain heart infusion broth for L. seeligeri). Optical density at 600 nm, corresponding to the number of bacteria, was collected for 16 h at 37 °C using a plate reader (Biotek Synergy H1). A code in R studio published by Qiu et al. was used to analyze the growth curves to determine bacteria viability. 40

Propidium Iodide Assay. *E. coli* or *B. subtilis*, prepared as described above, was washed three times with 0.85% NaCl followed by three washes with 2 mM HEPES 25 mM NaCl (pH 7.2). Bacteria were then mixed with the desired volume of NPs to reach a final incubation concentration of 1×10^8 cfu/mL. Particles and bacteria were incubated for 2 h at 37 °C while being shaken at 280 rpm. After incubation, propidium iodide was added to the bacteria—particle suspension (2 μ M final concentration) and allowed to mix for 30 min. After staining, 10μ L of suspension was then sandwiched between a

coverslip and microscope slide for fluorescence imaging. Fluorescence and differential interference contrast images were acquired using a Nikon Ti-E inverted microscope equipped with a $100 \times /1.49 \text{NA}$ TIRF oil-immersion objective.

Vancomycin-BODIPY and Propidium Iodine Double Staining. Vancomycin-BODIPY was first dissolved in DMSO and then in DI water to prepare a stock solution of 30 μ M. The stock solution was added to *E. coli* cells to a working concentration of 1 μ M. Propidium iodine stock solution was subsequently added to the same *E. coli* samples to a working concentration of 2 μ M. Cells were incubated with both dyes at 37 °C for 30 min, followed by three washing steps using 2 mM HEPES buffer containing 25 mM NaCl. After washing, cells were imaged immediately.

Scanning Electron Microscopy. E. coli $(1 \times 10^8 \text{ cfu/mL})$ and col/pho Janus NPs (128 pM) were mixed and incubated in 2 mM HEPES 25 mM NaCl (pH 7.2) for 2 h at 37 °C with 280 rpm shaking. A portion of the mixture was subsequently added to a cleaned glass coverslip and allowed to settle to the surface for 30 min. After this, Karnovsky's fixative (2% paraformaldehyde and 2.5% glutaraldehyde in 100 mM Sorenson's phosphate buffer) was gently added to the coverslip, and the sample was stored at 4 °C overnight. The next day, the fixative was removed by washing the sample twice with Sorenson's phosphate buffer. The bacterial sample was postfixed with 1% (v/v) osmium tetroxide for 90 min at room temperature, followed by four washes using ultrapure water. The sample was then dehydrated using a series of ethanol/water mixtures with increasing ethanol fraction [35%, 50%, 75%, and 95% ethanol (v/v in water)]. Each wash was done twice with 15 min of incubation. The sample was finally washed in pure ethanol three times for 20 min each time. The dehydrated sample was then washed twice with hexamethyldisilazane for 10 min each and transferred to a desiccator to dry overnight. A 5 nm thick layer of Au/Pd alloy was sputter-coated onto the surface of each sample. The sample was then imaged using an FEI Quanta 600 scanning electron microscope in high-vacuum mode (Nanoscale Characterization Facility at Indiana University).

Reactive Oxygen Species. *E. coli* or *B. subtilis* was washed three times with 0.85% NaCl followed by three washes with 2 mM HEPES and 25 mM NaCl (pH 7.2). For experiments with particles, bacteria $(1 \times 10^8 \text{ cfu/mL})$ were incubated with 64 pM col/pho JPs for 2 h at 37 °C while being shaken at 280 rpm. Buffer was used as a blank for samples without NPs. After incubation, CellROX (5 μ M final concentration) was added to the bacteria–particle suspension and mixed for 30 min. After staining, 10 μ L of suspension was then sandwiched between a coverslip and microscope slide for fluorescence imaging. Fluorescence and differential interference contrast images were acquired using a Nikon Ti-E inverted microscope equipped with a $100\times/1.49$ NA TIRF oil-immersion objective.

COMPUTATIONAL MODELS AND METHODS

MARTINI Force Field Descriptions. The implementation of CGMD simulations was performed using the 2023 version of GROMACS.⁴⁴ In the MARTINI force field,³⁸ atoms are represented by CG beads. Each bead corresponds to up to four heavy atoms and is categorized into one of four types: polar, nonpolar, apolar, or charged. These types are denoted by the labels P, N, C, and Q, respectively. Figure 3a, Figures S8–S9, and Tables S1–S2 provide details on the bead types used for Janus NP models and lipids in the present study.

Models of Janus NP. In our simulation, we used two Janus NP models: +/pho JP and col/pho JP (Figure 3a). The +/pho JP model was adapted from our previous works. ^{30,33} The Janus NP's gold (Au) core was constructed using a bulk face-centered cubic (FCC) lattice with a constant of 0.408 nm, and the diameter of the Au core was chosen to be 10 nm, which is larger than the thickness of the lipid bilayer. The Au core was constructed by using inert metal beads C5. The NP's surface was divided into two distinct regions: a hydrophilic hemisphere

and a hydrophobic hemisphere. The hydrophilic hemisphere of the +/pho IP model was covered with positively charged hydrophilic beads (Qd) with an areal density of 2.5 nm⁻², while the hydrophilic hemisphere of the col/pho JP model was covered with colistin with an areal density of 1.0 nm⁻². Each colistin molecule's lipid tail was connected to the Au core via a sulfur bead (N0). We utilized the CG representation of colistin from Lei Fu et al.,³⁹ and the list of CG beads for colistin is presented in Figure S8 and Table S1. In both Janus designs, the hydrophobic hemisphere was covered with sulfur beads (N0) at an areal density of 4.7 nm⁻². Each N0 bead was bonded with a hydrophobic alkyl chain represented by four C1 beads to mimic the octadecane carbon chain. To ensure the core's rigidity, we treated the interactions between the Au beads in the core with harmonic bond potentials using a force constant of 10000 kJ mol⁻¹. The Au-Qd and Au-N0 interactions were applied with a force constant of 6400 kJ mol⁻¹ and an equilibrium bond length of 0.24 nm. The interactions between the sulfur beads with the alkyl chain and the lipid tail of colistin were applied with a harmonic bond potential force constant of 1250 kJ mol⁻¹ and an equilibrium bond length of 0.47 nm. Additionally, we applied a harmonic bond potential force constant of 1250 kJ mol⁻¹ with an equilibrium bond length of 0.47 nm and a cosine angle potential of 180° with a force constant of 25 kJ mol⁻¹ to the bonds in the ligand. We used the bond, angle, and dihedral parameters of colistin from Lei Fu et al.³⁹

Model of Bacterial-Mimicking Membrane. A bacterialmimicking membrane model was constructed using the CHARMM-GUI web site, 45,46 consisting of a combination of rough lipopolysaccharide (RaLPS) and 1-palmitoyl-2-oleoylsn-glycero-3-phosphocholine (POPC). The RaLPS/POPC membrane was initially generated with a specific ratio of input lipids using the MARTINI membrane builder tool within CHARMM-GUI, with the CG beads of POPC (Figure S9a) and RaLPS (Figure S9b and Table S2). In this study, a molar ratio of 40:60 RaLPS to POPC was used in the simulation to ensure a surface coverage of RaLPS of about 75% (Figure S10a), as reported for bacterial outer membranes. 47,48 The total number of CG lipids and waters in the RaLPS/POPC membranes were 1500 and ~235000, respectively, and the membrane dimension was about $30 \times 30 \text{ nm}^2$. To equilibrate the membrane, energy minimization was performed with steepest descent for 5000 steps, followed by subsequent isothermal-isobaric (NPT) equilibration simulations. The number of particles (N), constant pressure (P), and temperature (T) were all kept constant with increasing time steps from 2.0 to 30 fs. A production simulation was then conducted for 6.0 μ s with a time step of 30 fs to fully relax the membrane (Figure S10b). Reaction-field electrostatics were used with a Coulomb cutoff of 1.1 nm and dielectric constants of 15 or 0 within or beyond this cutoff distance, respectively. Lennard-Jones (LJ) interactions were cut off at 1.1 nm, shifting the potential energy to zero. The temperature was maintained at a constant 310 K via separate coupling of the solvent (water) and lipid components to a v-rescaling thermostat with a relaxation time of 1.0 ps. Pressure was semi-isotropically coupled at 1.0 bar, with the Berendsen scheme used for the NPT equilibration with relaxation time and compressibility of 12.0 ps and 3×10^{-4} bar⁻¹, respectively. After equilibration, the Parrinello-Rahman barostat was used for a long production run.

Dynamics Simulation of Janus NP Interacting with the RaLPS/POPC Membrane. The dynamics of Janus NP interacting with the RaLPS/POPC membrane was subjected to a series of MD simulation steps. The simulation began by positioning the NP above the middle plane of the bilayer with two parts of the NP facing toward the membrane (Figure 3c at 0 ns). A steepest descent minimization procedure, consisting of 10000 steps, was then applied to resolve any steric clashes. After minimization, the Janus NP was pulled toward the membrane and restrained at a COM distance of 6.0 nm between the particle and membrane for 100 ns. Further free dynamics runs were then performed for a total of 2.0 μ s. The time step for Janus NP-membrane interaction simulations was set at 20 fs. Reaction-field electrostatics were used with a Coulomb cutoff of 1.4 nm and dielectric constants of 15 or 0 within or beyond this cutoff distance, respectively. The LJ force field was cut off at 1.4 nm, and the potential energy was shifted to zero. NPT ensembles were used to control the temperature and pressure of the system. Constant temperature was maintained at 310 K via separate coupling of the solvent (water), lipids in the membrane, and the Janus NP to vrescaling thermostats with a relaxation time of 1.0 ps. The pressure was semi-isotropically coupled at 1.0 bar and controlled by the Berendsen barostat with a relaxation time of 12.0 ps and compressibility of $3 \times 10^{-4} \text{ bar}^{-1}$.

Potential Mean Force Simulations. To investigate the binding energy of two designs of Janus NP to the RaLPS/POPC membrane, we utilized the PMF profile achieved through the umbrella sampling technique.⁴⁹ Our simulation method involved pulling the Janus NP toward the membrane in the z-direction, with the distance between the center-of-mass (COM) of the particle and the center of the membrane specified as the reaction coordinate (variable). To sample the distance in the range of 8.0–11.5 nm, we used windows of 0.2 nm width and applied an umbrella harmonic potential with a force constant of 1000 kJ mol⁻¹ nm⁻². For each window, we conducted equilibration and production runs with simulation times of 50 and 100 ns, respectively.

MD Result Analysis. To analyze the membrane defects caused by Janus NPs, we monitored the reduction in the membrane area (Figure 3d). Using the gmx energy tool, we extracted the dimensions of the lipid bilayer throughout the simulation. Also, in Figure 3d, we used gmx energy to calculate the average Coulomb interaction between the Janus NP and the lipids in the membrane. To calculate the average order parameters of the lipid tails in the membrane (Figure S10b), we used a custom Python script (do-ordered-gmx5.py), which can be found elsewhere. 50 Specifically, the lipid order parameters were defined as $S_{CC} = 0.5 \times (3 \cos^2 \theta - 1)$, where θ represents the angle between the bond formed by two coarse-grained beads and the bilayer normal (Figure S10b). To extract PMF profiles (Figure 3e), we utilized the Weighted Histogram Analysis Method (WHAM),⁵¹ which is included in GROMACS as the wham utility. We determined the binding energy as the difference between the highest and lowest values in the PMF curve. Snapshots during the simulation were rendered using the Visual Molecular Dynamics (VMD) software.52

ASSOCIATED CONTENT

Supporting Information

The Supporting Information is available free of charge at https://pubs.acs.org/doi/10.1021/acsanm.3c04486.

Effect of +/pho Janus NPs on *E. coli* viability assessed using propidium iodine assay, the effect of imaging buffer on propidium iodine staining of *E. coli*, the effect of soluble colistin on free colistin on the viability of *E. coli*, the vancomycin-BODIPY labeling of *E. coli*, the effect of soluble colistin on free colistin on the viability of *V. cholera*, propidium iodide staining of *B. subtilis*, characterization of dendrimer NPs, CG representation of the polycationic ligand colistin, CG representation of POPC and RaLPS, modeling of 40 mol % RaLPS/POPC membrane that gives a surface coverage of RaLPS of 75%, CG bead types of colistin, CG bead types of RaLPS from CHARM-GUI, captions for Videos S1 and S2 (PDF)

Video S1: CGMD simulation of the interaction between the col/pho Janus NP and the RaLPS/POPC membrane for 2.00 μ s (AVI)

Video S2: CGMD simulation of the interaction between the +/pho Janus NP and the RaLPS/POPC membrane for 2.00 μ s (AVI)

AUTHOR INFORMATION

Corresponding Author

Yan Yu — Department of Chemistry, Indiana University, Bloomington, Indiana 47405, United States; ⊚ orcid.org/ 0000-0001-6496-5045; Email: yy33@indiana.edu

Authors

Jared T. Wiemann – Department of Chemistry, Indiana University, Bloomington, Indiana 47405, United States; orcid.org/0000-0003-3416-0558

Danh Nguyen – Department of Mechanical Engineering, University of Wisconsin—Madison, Madison, Wisconsin 53706, United States

Swagata Bhattacharyya – Department of Chemistry, Indiana University, Bloomington, Indiana 47405, United States

Ying Li — Department of Mechanical Engineering, University of Wisconsin—Madison, Madison, Wisconsin 53706, United States; ⊚ orcid.org/0000-0002-1487-3350

Complete contact information is available at: https://pubs.acs.org/10.1021/acsanm.3c04486

Author Contributions

J.T.W. and Y.Y. conceived the idea and designed the experiments, and D.N. and Y.L. designed the simulations. J.T.W. and S.B. performed all experiments and related data analysis. D.N. performed all simulations and related analysis. J.T.W., D.N., S.B., Y.L., and Y.Y. wrote the manuscript. All authors have given approval to the final version of the manuscript.

Notes

The authors declare no competing financial interest.

ACKNOWLEDGMENTS

We thank Prof. J. P. Gerdt at Indiana University and Prof. Andrew Camilli at Tufts University for providing bacterial cultures used in this study, and Dr. Yi Yi and Dr. Jun Chen at IUB Nanoscale Characterization Facility for assistance with instrument use. This work was supported by the National Science Foundation under Grant 2153891 (to Y.Y. and Y.L.). Y.L. was partially supported by the US National Science Foundation under Grants OAC-2326802 and CBET-2313754.

REFERENCES

- (1) Anonymous, Antibiotic resistance threats in the United States, 2019.
- (2) Gao, W.; Zhang, L. Nanomaterials arising amid antibiotic resistance. *Nature Reviews Microbiology* **2021**, *19*, 1–2.
- (3) Makabenta, J. M. V.; et al. Nanomaterial-based therapeutics for antibiotic-resistant bacterial infections. *Nature Reviews Microbiology* **2021**, *19*, 1–14.
- (4) Linklater, D. P.; et al. Mechano-bactericidal actions of nanostructured surfaces. *Nature Reviews Microbiology* **2021**, *19*, 1–15.
- (5) Gupta, A.; Mumtaz, S.; Li, C.-H.; Hussain, I.; Rotello, V. M. Combatting antibiotic-resistant bacteria using nanomaterials. *Chem. Soc. Rev.* 2019, 48, 415–427.
- (6) Zheng, K.; Setyawati, M. I.; Leong, D. T.; Xie, J. Antimicrobial silver nanomaterials. *Coord. Chem. Rev.* **2018**, *357*, 1–17.
- (7) Díez-Pascual, A. M. Antibacterial Activity of Nanomaterials; Multidisciplinary Digital Publishing Institute: 2018.
- (8) Zhao, Y.; et al. Small Molecule-Capped Gold Nanoparticles as Potent Antibacterial Agents That Target Gram-Negative Bacteria. *J. Am. Chem. Soc.* **2010**, *132*, 12349–12356.
- (9) Hang, M. N.; et al. Impact of Nanoscale Lithium Nickel Manganese Cobalt Oxide (NMC) on the Bacterium Shewanella oneidensis MR-1. *Chem. Mater.* **2016**, 28, 1092–1100.
- (10) Feng, Z. V.; et al. Biological impact of nanoscale lithium intercalating complex metal oxides to model bacterium B. subtilis. *Environmental Science: Nano* **2019**, *6*, 305–314.
- (11) Arakha, M.; et al. Antimicrobial activity of iron oxide nanoparticle upon modulation of nanoparticle-bacteria interface. *Sci. Rep.* **2015**, *S*, 14813.
- (12) Natan, M.; Gutman, O.; Lavi, R.; Margel, S.; Banin, E. Killing Mechanism of Stable N-Halamine Cross-Linked Polymethacrylamide Nanoparticles That Selectively Target Bacteria. *ACS Nano* **2015**, *9*, 1175–1188.
- (13) Nederberg, F.; et al. Biodegradable nanostructures with selective lysis of microbial membranes. *Nat. Chem.* **2011**, *3*, 409–414.
- (14) Mei, L.; Lu, Z.; Zhang, X.; Li, C.; Jia, Y. Polymer-Ag Nanocomposites with Enhanced Antimicrobial Activity against Bacterial Infection. ACS Appl. Mater. Interfaces 2014, 6, 15813—15821.
- (15) Rai, A.; et al. One-step synthesis of high-density peptide-conjugated gold nanoparticles with antimicrobial efficacy in a systemic infection model. *Biomaterials* **2016**, *85*, 99–110.
- (16) Linklater, D. P.; et al. Antibacterial Action of Nanoparticles by Lethal Stretching of Bacterial Cell Membranes. *Adv. Mater.* **2020**, 32, No. e2005679.
- (17) Caudill, E. R.; et al. Wall teichoic acids govern cationic gold nanoparticle interaction with Gram-positive bacterial cell walls. *Chemical Science* **2020**, *11*, 4106–4118.
- (18) Berry, V.; Gole, A.; Kundu, S.; Murphy, C. J.; Saraf, R. F. Deposition of CTAB-Terminated Nanorods on Bacteria to Form Highly Conducting Hybrid Systems. *J. Am. Chem. Soc.* **2005**, *127*, 17600–17601.
- (19) Buchman, J. T.; et al. Using an environmentally-relevant panel of Gram-negative bacteria to assess the toxicity of polyallylamine hydrochloride-wrapped gold nanoparticles. *Environmental Science:* Nano 2018, 5, 279–288.
- (20) Hayden, S. C.; et al. Aggregation and Interaction of Cationic Nanoparticles on Bacterial Surfaces. *J. Am. Chem. Soc.* **2012**, *134*, 6920–6923.
- (21) Feng, Z. V.; et al. Impacts of gold nanoparticle charge and ligand type on surface binding and toxicity to Gram-negative and Gram-positive bacteria. *Chemical Science* **2015**, *6*, 5186–5196.
- (22) Li, X.; et al. Functional Gold Nanoparticles as Potent Antimicrobial Agents against Multi-Drug-Resistant Bacteria. ACS Nano 2014, 8, 10682–10686.
- (23) Shebl, R. I.; Farouk, F.; Azzazy, H. M. E.-S. Effect of Surface Charge and Hydrophobicity Modulation on the Antibacterial and Antibiofilm Potential of Magnetic Iron Nanoparticles. *J. Nanomater.* **2017**, 2017, 3528295.

- (24) Ahmad Nor, Y.; et al. Shaping Nanoparticles with Hydrophilic Compositions and Hydrophobic Properties as Nanocarriers for Antibiotic Delivery. ACS central science 2015, 1, 328–334.
- (25) Zheng, K.; Setyawati, M. I.; Leong, D. T.; Xie, J. Surface Ligand Chemistry of Gold Nanoclusters Determines Their Antimicrobial Ability. *Chem. Mater.* **2018**, *30*, 2800–2808.
- (26) Huo, S.; et al. Fully Zwitterionic Nanoparticle Antimicrobial Agents through Tuning of Core Size and Ligand Structure. *ACS Nano* **2016**, *10*, 8732–8737.
- (27) Lee, K.; Yu, Y. Lipid bilayer disruption induced by amphiphilic Janus nanoparticles: the non-monotonic effect of charged lipids. *Soft Matter* **2019**, *15*, 2373–2380.
- (28) Lee, K.; Zhang, L.; Yi, Y.; Wang, X.; Yu, Y. Rupture of Lipid Membranes Induced by Amphiphilic Janus Nanoparticles. *ACS Nano* **2018**, *12*, 3646–3657.
- (29) Lee, K.; Yu, Y. Lipid Bilayer Disruption by Amphiphilic Janus Nanoparticles: The Role of Janus Balance. *Langmuir* **2018**, *34*, 12387–12393.
- (30) Wiemann, J. T.; Shen, Z.; Ye, H.; Li, Y.; Yu, Y. Membrane poration, wrinkling, and compression: deformations of lipid vesicles induced by amphiphilic Janus nanoparticles. *Nanoscale* **2020**, *12*, 20326–20336.
- (31) Chen, K. L.; Bothun, G. D. Nanoparticles Meet Cell Membranes: Probing Nonspecific Interactions using Model Membranes. *Environ. Sci. Technol.* **2014**, *48*, 873–880.
- (32) Su, C. F.; Merlitz, H.; Rabbel, H.; Sommer, J. U. Nanoparticles of Various Degrees of Hydrophobicity Interacting with Lipid Membranes. *J. Phys. Chem. Lett.* **2017**, *8*, 4069–4076.
- (33) Wiemann, J. T.; Nguyen, D.; Li, Y.; Yu, Y. Domain-selective disruption and compression of phase-separated lipid vesicles by amphiphilic Janus nanoparticles. *iScience* **2022**, *25*, 105525.
- (34) Sabnis, A.; et al. Colistin kills bacteria by targeting lipopolysaccharide in the cytoplasmic membrane. *eLife* **2021**, *10*, No. e65836.
- (35) El-Sayed Ahmed, M. A. E.-G.; et al. Colistin and its role in the Era of antibiotic resistance: an extended review (2000–2019). *Emerging Microbes & Infections* **2020**, *9*, 868–885.
- (36) Štokes, J. M.; et al. Cold Stress Makes Escherichia coli Susceptible to Glycopeptide Antibiotics by Altering Outer Membrane Integrity. *Cell Chemical Biology* **2016**, 23, 267–277.
- (37) Zhang, B.; et al. Synthesis of vancomycin fluorescent probes that retain antimicrobial activity, identify Gram-positive bacteria, and detect Gram-negative outer membrane damage. *Communications Biology* **2023**, *6*, 409.
- (38) Marrink, S. J.; Risselada, H. J.; Yefimov, S.; Tieleman, D. P.; de Vries, A. H. The MARTINI Force Field: Coarse Grained Model for Biomolecular Simulations. *J. Phys. Chem. B* **2007**, *111*, 7812–7824.
- (39) Fu, L.; Wan, M.; Zhang, S.; Gao, L.; Fang, W. Polymyxin B Loosens Lipopolysaccharide Bilayer but Stiffens Phospholipid Bilayer. *Biophys. J.* **2020**, *118*, 138–150.
- (40) Qiu, T. A.; et al. Growth-Based Bacterial Viability Assay for Interference-Free and High-Throughput Toxicity Screening of Nanomaterials. *Anal. Chem.* **2017**, *89*, 2057–2064.
- (41) Behera, N.; et al. Oxidative stress generated at nickel oxide nanoparticle interface results in bacterial membrane damage leading to cell death. RSC Adv. 2019, 9, 24888–24894.
- (42) Sampson, T. R.; et al. Rapid Killing of Acinetobacter baumannii by Polymyxins Is Mediated by a Hydroxyl Radical Death Pathway. *Antimicrob. Agents Chemother.* **2012**, *56*, 5642–5649.
- (43) Lopez, A. I.; Reins, R. Y.; McDermott, A. M.; Trautner, B. W.; Cai, C. Antibacterial activity and cytotoxicity of PEGylated poly-(amidoamine) dendrimers. *Molecular BioSystems* **2009**, *5*, 1148–1156.
- (44) Bekker, H.; et al. Gromacs: A parallel computer for molecular dynamics simulations. *Physics Computing* **1993**, *92*, 252–256.
- (45) Jo, S.; Kim, T.; Iyer, V. G.; Im, W. CHARMM-GUI: A webbased graphical user interface for CHARMM. *J. Comput. Chem.* **2008**, 29, 1859–1865.
- (46) Lee, J.; et al. CHARMM-GUI Input Generator for NAMD, GROMACS, AMBER, OpenMM, and CHARMM/OpenMM Simu-

- lations Using the CHARMM36 Additive Force Field. J. Chem. Theory Comput. 2016, 12, 405-413.
- (47) Klein, G.; Raina, S. Regulated Assembly of LPS, Its Structural Alterations and Cellular Response to LPS Defects. *Int. J. Mol. Sci.* **2019**, *20*, 356.
- (48) Rodriguez-Loureiro, I.; Latza, V. M.; Fragneto, G.; Schneck, E. Conformation of Single and Interacting Lipopolysaccharide Surfaces Bearing O-Side Chains. *Biophys. J.* **2018**, *114*, 1624–1635.
- (49) Lemkul, J. A.; Bevan, D. R. Assessing the Stability of Alzheimer's Amyloid Protofibrils Using Molecular Dynamics. *J. Phys. Chem. B* **2010**, *114*, 1652–1660.
- (50) Kets de Vries, M. F. R. Do-order tool, 2017.
- (51) Kumar, S.; Rosenberg, J. M.; Bouzida, D.; Swendsen, R. H.; Kollman, P. A. THE weighted histogram analysis method for free-energy calculations on biomolecules. I. The method. *J. Comput. Chem.* **1992**, *13*, 1011–1021.
- (52) Humphrey, W.; Dalke, A.; Schulten, K. VMD: Visual molecular dynamics. *J. Mol. Graphics* **1996**, *14*, 33–38.